Performance Comparison of Nodally Integrated Galerkin Meshfree Methods and Nodally Collocated Strong Form Meshfree Methods

M. Hillman and J.S. Chen

Abstract For a truly meshfree technique, Galerkin meshfree methods rely chiefly on nodal integration of the weak form. In the case of Strong Form Collocation meshfree methods, direct collocation at the nodes can be employed. In this paper, performance of these node-based Galerkin and collocation meshfree methods is compared in terms of accuracy, efficiency, and stability. Considering both accuracy and efficiency, the overall effectiveness in terms of CPU time versus error is also assessed. Based on the numerical experiments, nodally integrated Galerkin meshfree methods with smoothed gradients and variationally consistent integration yield the most effective solution technique, while direct collocation of the strong form at nodal locations has comparable effectiveness.

1 Introduction

There are several attractive features of both Galerkin- and Strong Form Collocation-based meshfree methods, each with their own drawbacks as well. In Galerkin-based methods, their implementation is similar to the finite element method (FEM). They have been shown to be effective for solving problems which are difficult for traditional FEMs [1–5], provide straight-forward *h*-adaptivity [6, 7], arbitrary order of smoothness, among many other unique properties that can be leveraged in solving PDEs [8]. On the other hand, special techniques are required to obtain optimal convergence without the employment of high-order quadrature [9]. If nodal integration is used, stabilization must also be employed [10]. Essential

M. Hillman
Department of Civil and Environmental Engineering,
The Pennsylvania State University, University Park, PA 16802-1408, USA

J.S. Chen (✉)
Department of Structural Engineering, University of California,
San Diego 9500 Gilman Drive, La Jolla, CA 92093-0085, USA
e-mail: js-chen@ucsd.edu

E. Oñate et al. (eds.), *Advances in Computational Plasticity*, Computational Methods in Applied Sciences 46, DOI 10.1007/978-3-319-60885-3_7

boundary conditions also need special treatment as well since meshfree methods do not in general possess the Kronecker delta property [11].

Nodal integration has been employed for quadrature in Galerkin meshfree methods for several reasons. Foremost, it maintains the meshfree characteristic of the method as opposed to using background meshes for integration. It also offers simplicity, efficiency, and ease of implementation. As such, the properties of solutions obtained by the Galerkin method with nodal integration have been thoroughly examined, and it is now well known that poor convergence and solution instability can be encountered when left untreated [9, 12–14]. The poor convergence is attributed to the inaccuracy in integrating the weak form [15], while the instability is due to the choice of quadrature locations which yield zero strain energy associated with sawtooth modes [10]. Several nodal integration methods have been developed to circumvent either of these problems, or both [12–14, 16–19]. Many methods are available which circumvent the stability issue such as residual-based methods [12, 13], stress points [10, 20, 21], Taylor expansion of strains [19, 22, 23], gradient-based approaches [24], or strain smoothing with divergence operation of the averaged integral [14]. The strain smoothing method can achieve both optimal convergence and solution stability. This technique was based on satisfaction of the so-called integration constraint [14], which was later generalized to the variational consistency conditions [9]. A method has been developed to satisfy these conditions by employing a Petrov-Galerkin formulation [9]. Recently, a two-level smoothing technique was developed to satisfy the quadratic constraints [25]. Several strategies exist to address other issues with domain integration, but are beyond the scope of discussion in this chapter.

The strong-form based collocation meshfree methods [26–28] are generally very simple to implement. They do not suffer from quadrature issues, nor do they require special techniques for enforcement of essential boundary conditions other than applying weights for optimal accuracy in the solution [29]. They also offer several of the attractive features of their Galerkin counterpart such as straightforward adaptive refinement. To the authors' knowledge, they do not suffer from spatial instability when nodal locations are employed as collocation points.

In the linearization of second order PDEs however, the implementation of collocation methods is not as straightforward as the Galerkin technique, since it requires third order derivatives of the approximation functions, which also increases computational cost. While collocation circumvents quadrature issues, a sufficient number of collocation points is still required for optimal convergence [28, 30]. The solution of second order PDEs in general requires second order derivatives which is not a negligible cost in local meshfree approximations such as the reproducing kernel [28], and quadratic accuracy is also required for convergence [28]. It should be noted that the former issue can be overcome by the employment of implicit gradient approximations [31].

Considering the benefits of each method along with their associated costs, a tradeoff exists and warrants examination. In this work, focus is on the class of nodally collocated strong form and nodally integrated weak form based meshfree methods. These two methods are of interest in that they both offer truly meshfree

solutions to PDEs. The Galerkin version requires quadrature treatment, so variationally consistent integration is employed. The tradeoff between efficiency and accuracy is examined, as well as the stability of the numerical solution. To present a unified analysis, we focus on the reproducing kernel approximation as a basis for these two methods.

This chapter is organized as follows. Section 2 gives an overview of the construction of the reproducing kernel approximation. A model problem and discussion of the solution by Strong Form Collocation and the Galerkin method are presented in Sect. 3, and techniques employed to obtain stable and convergent solutions in nodal integration of the Galerkin method are also given. Section 4 presents several numerical examples, and compares the convergence rates, effectiveness (CPU time versus error), and stability of the two methods. The several conclusions that can be drawn from the study are given in Sect. 5.

2 Reproducing Kernel Approximation

Let a domain $\overline{\Omega} = \Omega \cup \partial\Omega$ be discretized by a set of N_P nodes $\mathcal{N} = \left\{ \mathbf{x}_1, \quad \cdots, \quad \mathbf{x}_{N_P} \,|\mathbf{x}_I \in \overline{\Omega} \right\}$ with corresponding node numbers $\mathcal{Z} = \{I|\mathbf{x}_I \in \mathcal{N}\}$. The nth order reproducing kernel (RK) approximation $u^h(\mathbf{x})$ of a function $u(\mathbf{x})$ is [1, 32]:

$$u^h(\mathbf{x}) \; = \sum_{I \in \mathcal{Z}} \Psi_I^{[n]}(\mathbf{x}) u_I \tag{1}$$

where $\{\Psi_I^{[n]}(\mathbf{x})\}_{I \in \mathcal{Z}}$ is the set of RK shape functions, and $\{u_I\}_{I \in \mathcal{Z}}$ are the associated coefficients. The shape functions $\Psi_I^{[n]}(\mathbf{x})$ are constructed by the product of a kernel function $\Phi_a(\mathbf{x} - \mathbf{x}_I)$ and a correction function $C^{[n]}(\mathbf{x}; \mathbf{x} - \mathbf{x}_I)$:

$$\Psi_I^{[n]}(\mathbf{x}) \; = \Phi_a(\mathbf{x} - \mathbf{x}_I) C^{[n]}(\mathbf{x}; \mathbf{x} - \mathbf{x}_I) \tag{2}$$

where

$$C^{[n]}(\mathbf{x}; \mathbf{x} - \mathbf{x}_I) = \{\mathbf{H}^{[n]}(\mathbf{x} - \mathbf{x}_I)\}^{\mathrm{T}} \mathbf{b}^{[n]}(\mathbf{x}). \tag{3}$$

In the above, $\mathbf{b}^{[n]}(\mathbf{x})$ and $\mathbf{H}^{[n]}(\mathbf{x} - \mathbf{x}_I)$ are column vectors of coefficients and nth order complete monomials, respectively. For example, for quadratic basis ($n = 2$) in two dimensions we have

$$\begin{aligned} \mathbf{b}^{[n]}(\mathbf{x}) &= \left[\mathrm{b}_{00}(\mathbf{x}) \quad \mathrm{b}_{10}(\mathbf{x}) \quad \mathrm{b}_{01}(\mathbf{x}) \quad \mathrm{b}_{20} \quad (\mathbf{x})\mathrm{b}_{11}(\mathbf{x}) \quad \mathrm{b}_{02}(\mathbf{x}) \right]^{\mathrm{T}}, \\ \mathbf{H}^{[n]}(\mathbf{x} - \mathbf{x}_I) &= \left[1 \quad x \quad y \quad x^2 \quad xy \quad y^2 \right]^{\mathrm{T}}. \end{aligned} \tag{4}$$

The kernel function $\Phi_a(\mathbf{x}-\mathbf{x}_I)$ has compact support with measure a, and the smoothness of the kernel is inherited by the approximation. For example, a kernel with C^2 continuity gives C^2 continuity of the approximation.

The coefficients $\mathbf{b}^{[n]}(\mathbf{x})$ are determined by enforcing the following reproducing conditions [3]:

$$\sum_{I\in\mathcal{Z}} \mathbf{H}^{[n]}(\mathbf{x}_I)\Psi_I^{[n]}(\mathbf{x}) \;= \mathbf{H}^{[n]}(\mathbf{x}). \tag{5}$$

With $\mathbf{b}^{[n]}(\mathbf{x})$ obtained from (5), the RK shape functions are constructed as

$$\Psi_I^{[n]}(\mathbf{x}) \;= \mathbf{H}^{[n]}(\mathbf{0})^{\mathrm{T}}\{\mathbf{M}^{[n]}(\mathbf{x})\}^{-1}\mathbf{H}^{[n]}(\mathbf{x}-\mathbf{x}_I)\Phi_a(\mathbf{x}-\mathbf{x}_I), \tag{6}$$

$$\mathbf{M}^{[n]}(\mathbf{x}) = \sum_{I\in\mathcal{Z}} \mathbf{H}^{[n]}(\mathbf{x}-\mathbf{x}_I)\{\mathbf{H}^{[n]}\}^{\mathrm{T}}(\mathbf{x}-\mathbf{x}_I)\Phi_a(\mathbf{x}-\mathbf{x}_I), \tag{7}$$

where $\mathbf{M}^{[n]}(\mathbf{x})$ is termed the *moment matrix*. The reproducing conditions (5) are met provided the moment matrix is invertible, which requires a sufficient number of nodes with non-zero cover over $\mathbf{x}$ that are not co-linear (in 2D), or co-planar (in 3-D) [33].

3 Solution to Boundary Value Problems by Galerkin and Strong Form Collocation Methods

3.1 Model Problem

Poisson's equation is considered for evaluating the relative performance of mesh-free Galerkin and Strong Form Collocation methods for the approximate solution of boundary value problems:

$$\begin{aligned} \nabla^2 u + s &= 0 \quad \text{in } \Omega \\ \nabla u\cdot\mathbf{n} &= h \quad \text{on } \partial\Omega_h \\ u &= g \quad \text{on } \partial\Omega_g \end{aligned} \tag{8}$$

where s, h and g are given values on the domain Ω, the natural boundary $\partial\Omega_h$, and essential boundary $\partial\Omega_g$, respectively, with $\partial\Omega_h \cap \partial\Omega_g = \varnothing$ and $\partial\Omega_h \cup \partial\Omega_g = \partial\Omega$.

3.2 Solutions Using the Strong Form Collocation Method

The basic approach of the Strong Form Collocation method is to approximate the solution of a boundary value problem by a finite dimensional space and strongly enforce zero residual of the PDE and boundary conditions at a number of points (called collocation points) in the domain and on the boundary of the domain.

Let the set of nodes $\mathcal{N}$ be decomposed into the sets $\mathcal{N}_d = \{\mathbf{x}_I | \mathbf{x}_I \in \Omega$, $\mathcal{N}_h = \{\mathbf{x}_I | \mathbf{x}_I \in \partial\Omega_h\}$, and $\mathcal{N}_g = \{\mathbf{x}_I | \mathbf{x}_I \in \partial\Omega_g\}$, with point numbers $\mathcal{Z}_h = \{I | \mathbf{x}_I \in \mathcal{N}_h\}$, $\mathcal{Z}_g = \{I | \mathbf{x}_I \in \mathcal{N}_g\}$, and $\mathcal{Z}_d = \{I | \mathbf{x}_I \in \mathcal{N}_d\}$, respectively. The enforcement of (8) at the set of nodes $\mathcal{N}$ using (1) as an approximation of u yields:

$$\begin{aligned} \sum_{I \in \mathcal{Z}} \nabla^2 \Psi_I(\mathbf{x}_L) u_I &= -s(\mathbf{x}_L), && L \in \mathcal{Z}_d, \\ \sum_{I \in \mathcal{Z}} \nabla \Psi_I(\mathbf{x}_L) u_I \bullet \mathbf{n}(\mathbf{x}_L) &= h(\mathbf{x}_L), && L \in \mathcal{Z}_h, \\ \sum_{I \in \mathcal{Z}} \Psi_I(\mathbf{x}_L) u_I &= g(\mathbf{x}_L), && L \in \mathcal{Z}_g. \end{aligned} \tag{9}$$

Figure 1 shows an example of the three sets of collocation points for the conditions in (9).

For implementation, a matrix version of (9) can be written as

$$\begin{aligned} \mathbf{A}\mathbf{u} &= \mathbf{b} \\ \mathbf{A} &= \left\{\mathbf{A}_d,\ \mathbf{A}_h,\ \mathbf{A}_g\right\}^{\mathrm{T}} \\ \mathbf{b} &= \left\{\mathbf{b}_d,\ \mathbf{b}_h,\ \mathbf{b}_g\right\}^{\mathrm{T}} \end{aligned} \tag{10}$$

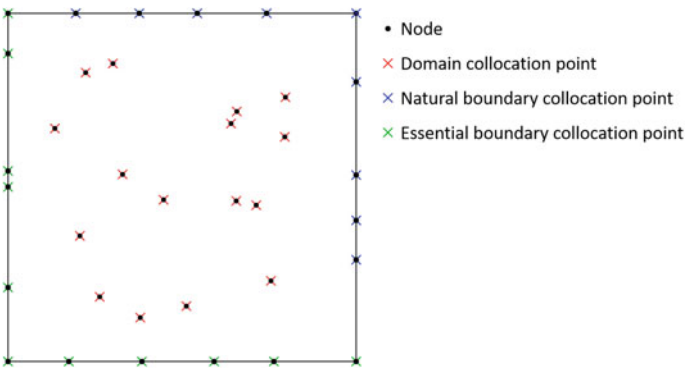

Fig. 1 Sets of collocation points for nodal collocation

where

$$\begin{aligned} [\mathbf{A}_d]_{IJ} &= \nabla^2 \Psi_J(\mathbf{x}_I), & [\mathbf{b}_d]_I &= s(\mathbf{x}_I), \quad I \subset \mathcal{Z}_d, \\ [\mathbf{A}_h]_{IJ} &= \nabla \Psi_J(\mathbf{x}_I) \bullet \mathbf{n}(\mathbf{x}_I), & [\mathbf{b}_h]_I &= h(\mathbf{x}_I), \quad I \subset \mathcal{Z}_h, \\ [\mathbf{A}_g]_{IJ} &= \Psi_J(\mathbf{x}_I), & [\mathbf{b}_g]_I &= g(\mathbf{x}_I), \quad I \subset \mathcal{Z}_g. \end{aligned} \tag{11}$$

The nodes used in the approximation of $u^h(\mathbf{x}_L)$ are termed *source points*. Typically, more collocation points are chosen than source points, and least-square methods are employed to solve the over-determined system. However, when the solution is collocated at the nodes themselves such as in (9), the number of collocation points and source points are equal and the system can be solved directly.

3.3 Solutions Using the Galerkin Method with Nodal Integration

The Galerkin method is based on solving the weak form of (8), which asks to find $u \in U$ such that for all $v \in V$ the following holds:

$$a(v,u) = L(v) \tag{12}$$

where $U = \{u | u \in H^1(\overline{\Omega}),\ u = g \text{ on } \partial\Omega_g\}$, $V = \{v | v \in H^1(\overline{\Omega}),\ v = 0 \text{ on } \partial\Omega_g\}$, and the bilinear and linear forms in (12) are

$$\begin{aligned} a(v,u) &\equiv \int_\Omega \nabla v(\mathbf{x}) \bullet \nabla u(\mathbf{x}) \mathrm{d}\Omega \\ L(v) = (v,s)_\Omega + (v,h)_{\partial\Omega_h} &\equiv \int_\Omega v(\mathbf{x}) s(\mathbf{x}) \mathrm{d}\Gamma + \int_{\partial\Omega_h} v(\mathbf{x}) h(\mathbf{x}) \mathrm{d}\Gamma. \end{aligned} \tag{13}$$

The Galerkin method introduces finite dimensional approximations $U^h \subset U$, and $V^h \subset V$, and seeks $u^h \in U^h$ for all $v^h \in V^h$ such that

$$a(v^h, u^h) = L(v^h). \tag{14}$$

Utilizing the RK approximation (1) for u^h and v^h:

$$\begin{aligned} u^h(\mathbf{x}) &= \sum_{I \in \mathcal{Z}} \Psi_I^{[n]}(\mathbf{x}) u_I, \\ v^h(\mathbf{x}) &= \sum_{I \in \mathcal{Z}} \Psi_I^{[n]}(\mathbf{x}) v_I, \end{aligned} \tag{15}$$

and the arbitrariness of $\{v_I\}_{I\in\mathcal{Z}}$, the matrix form of (14) is

$$\mathbf{K}\mathbf{u}=\mathbf{f} \tag{16}$$

where $\mathbf{u}$ is the column vector of coefficients $\{u_I\}_{I\in\mathcal{Z}}$, and $\mathbf{K}$ and $\mathbf{f}$ are the stiffness matrix and force column vector defined as

$$\begin{aligned}\mathbf{K} &= \int_\Omega \mathbf{B}^{\mathrm{T}}(\mathbf{x})\mathbf{B}(\mathbf{x})\mathrm{d}\Omega\\ \mathbf{f} &= \mathbf{f}_s + \mathbf{f}_h \equiv \int_\Omega \mathbf{N}^{\mathrm{T}}(\mathbf{x})s(\mathbf{x})d\Gamma + \int_{\partial\Omega_h} \mathbf{N}^{\mathrm{T}}(\mathbf{x})h(\mathbf{x})\mathrm{d}\Gamma\end{aligned} \tag{17}$$

where

$$\begin{aligned}\mathbf{B}(\mathbf{x}) &= \begin{bmatrix} \Psi_{1,1}(\mathbf{x}) & \Psi_{2,1}(\mathbf{x}) & \dots & \Psi_{N_P,1}(\mathbf{x}) \\ \vdots & & & \\ \Psi_{1,d}(\mathbf{x}) & \Psi_{2,d}(\mathbf{x}) & \dots & \Psi_{N_P,d}(\mathbf{x}) \end{bmatrix},\\ \mathbf{N}(\mathbf{x}) &= [\,\Psi_1(\mathbf{x}) \quad \Psi_2(\mathbf{x}) \quad \dots \quad \Psi_{N_P}(\mathbf{x})\,],\end{aligned} \tag{18}$$

and $(\cdot)_{,i} \equiv \partial(\cdot)/\partial x_i$.

Domain integration performed using the nodes as integration points is shown in Fig. 2a, where integration points coincide with the nodes has been termed *direct nodal integration* (DNI) in the literature. The nodal integration of the Galerkin equation (16) yields a stiffness matrix and force vector evaluated as

$$\begin{aligned}\mathbf{K} &= \sum_{L\in\mathcal{Z}} \mathbf{B}^{\mathrm{T}}(\mathbf{x}_L)\mathbf{B}(\mathbf{x}_L)W_L\\ \mathbf{f} &= \sum_{L\in\mathcal{Z}} \mathbf{N}^{\mathrm{T}}(\mathbf{x}_L)s(\mathbf{x}_L)W_L + \sum_{L\in\mathcal{Q}} \mathbf{N}^{\mathrm{T}}(\mathbf{x}_L)h(\mathbf{x}_L)S_L\end{aligned} \tag{19}$$

where $\{W_L\}_{L\in\mathcal{Z}}$ are nodal quadrature weights, $\mathcal{Q}$ is the set of indices of quadrature points on the natural boundary, and $\{S_L\}_{L\in\mathcal{Q}}$ is the set of associated quadrature weights.

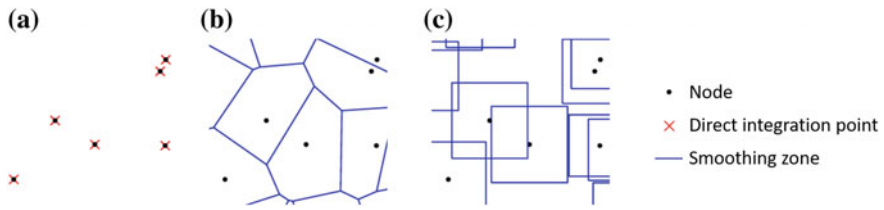

Fig. 2 Integration methods for (**a**) direct nodal integration, (**b**) SCNI integration, and (**c**) SNNI integration

This method does not attain optimal convergence rates in most situations due to the inherent low-order quadrature of this scheme. In addition, the choice of nodes as integration points severely underestimates the strain energy of low energy modes and the solution is subject to rank instability. Because of this, stabilized and corrected methods are usually employed with nodal integration.

To improve the accuracy of nodal integration, the work in [14] derived the following requirement on the approximation space and numerical integration at hand to attain linear exactness (passing the linear patch test) in the Galerkin solution of second order PDEs:

$$\hat{\int_{\Omega_L}} \nabla \Psi_I(\mathbf{x}) \mathrm{d}\Omega = \hat{\int_{\partial\Omega_L}} \Psi_I(\mathbf{x}) \mathbf{n}(\mathbf{x}) \mathrm{d}\Gamma \qquad \forall I \tag{20}$$

where "^" denotes numerical integration and $\{\Psi_I(\mathbf{x})\}_{I \in \mathcal{Z}}$ are shape functions with linear completeness. A stabilized conforming nodal integration (SCNI) has been proposed [14] which employs a smoothed gradient $\tilde{\nabla}$ of the RK approximation (1), calculated in each nodal representative domain Ω_L by

$$\tilde{\nabla} u^h(\mathbf{x}_L) = \frac{1}{W_L} \int_{\Omega_L} \nabla u^h(\mathbf{x}) \mathrm{d}\Omega = \frac{1}{W_L} \int_{\partial\Omega_L} u^h(\mathbf{x}) \mathbf{n}(\mathbf{x}) \mathrm{d}\Gamma \tag{21}$$

where $W_L = |\Omega_L|$. The nodal domains partition the total domain in a conforming fashion, as shown in Fig. 2b, which yields a method that satisfies (20). Because of the fact first order derivatives are not directly evaluated at the nodes, the zero energy modes in direct nodal integration do not appear in the solution by SCNI, thus addressing both issues with direct nodal integration. When linear bases are employed in (21), the method attains the optimal convergence rate consistent with the linear completeness in the approximation.

Employing the smoothed gradients in (21), the SCNI method can be phrased as

$$\widetilde{\mathbf{K}}\mathbf{u} = \mathbf{f} \tag{22}$$

where

$$\widetilde{\mathbf{K}} = \sum_{L \in \mathcal{Z}} \tilde{\mathbf{B}}^{\mathrm{T}}(\mathbf{x}_L) \tilde{\mathbf{B}}(x_L) W_L,$$
$$\tilde{\mathbf{B}}(\mathbf{x}_L) = \begin{bmatrix} \tilde{b}_{11}(\mathbf{x}_L) & \tilde{b}_{21}(\mathbf{x}_L) & \dots & \tilde{b}_{N_P x}(\mathbf{x}_L) \\ \vdots & & & \\ \tilde{b}_{1d}(\mathbf{x}_L) & \tilde{b}_{2d}(\mathbf{x}_L) & \dots & \tilde{b}_{N_P d}(\mathbf{x}_L) \end{bmatrix}, \quad \tilde{b}_{Ii}(\mathbf{x}_L) = \frac{1}{W_L} \int_{\partial\Omega_L} \Psi_I(\mathbf{x}) n_i(\mathbf{x}) \mathrm{d}\Gamma. \tag{23}$$

A stabilized non-conforming nodal integration (SNNI) has also been proposed [24] where the smoothing domains do not conform:

$$\tilde{\nabla} u^h(\mathbf{x}_L) = \frac{1}{\overline{W}_L} \int_{\overline{\Omega}_L} \nabla u^h(\mathbf{x}) \mathrm{d}\Omega = \frac{1}{\overline{W}_L} \int_{\partial \overline{\Omega}_L} u^h(\mathbf{x}) \mathbf{n}(\mathbf{x}) \mathrm{d}\Gamma \tag{24}$$

where $\overline{\Omega}_L$ is a non-conforming smoothing domain, and $\overline{W}_L = |\overline{\Omega}_L|$. The set of nodal domains can be constructed by using boxes for example, as shown in Fig. 2c. This method fails to pass the patch test because of the simplification, but can be corrected with the methods discussed below.

Recently, the conditions in (20) were extended to nth order constraints, with the general framework termed variational consistency [9]. Assuming nth order completeness of the trial functions, the divergence criteria in (20) can be cast in a more general fashion that reduces to the integration constraints for linear solutions:

$$\int_{\Omega}^{\wedge} \widehat{\Psi}^{[n]}_{I,i}(\mathbf{x}) \{\mathbf{H}^{[n-1]}\}^{\mathrm{T}}(\mathbf{x}) \mathrm{d}\Omega = \int_{\partial\Omega}^{\wedge} \widehat{\Psi}^{[n]}_{I}(\mathbf{x}) \mathbf{H}^{[n-1]}(\mathbf{x}) n_i(\mathbf{x}) \mathrm{d}\Gamma - \int_{\Omega}^{\wedge} \widehat{\Psi}^{[n]}_{I}(\mathbf{x}) \mathbf{H}^{[n-1]}_{,i}(\mathbf{x}) \mathrm{d}\Omega \quad \forall I \tag{25}$$

where $\{\widehat{\Psi}^{[n]}_I(\mathbf{x})\}_{I \in \mathcal{Z}}$ are shape functions associated with the test function space. The reduction in the order of complete monomials to $n-1$ that appear in the above equation is a result of solving the weak form of a second order PDE with integration by parts.

Leveraging the fact that nth order completeness by the trial space and satisfaction of the nth order integration constraints (25) by the test space are needed to satisfy nth order variational consistency, a Petrov-Galerkin method can be employed where test and trial functions are constructed to play different roles in the Galerkin solution of PDEs. In [9], an assumed test function gradient was introduced in order to satisfy the variational consistency conditions:

$$\begin{aligned} u^h_{,i}(\mathbf{x}) &= \sum_{I=1}^{N_P} \Psi^{[n]}_{I,i}(\mathbf{x}) u_I, \\ v^h_{,i}(\mathbf{x}) &= \sum_{I=1}^{N_P} \widehat{\Psi}^{[n]}_{I,i}(\mathbf{x}) v_I. \end{aligned} \tag{26}$$

The test function gradient can be constructed using the trial shape functions with an additional set of bases $\mathbf{H}^{[n-1]}(\mathbf{x})$ with constant coefficients $\boldsymbol{\xi}_{Ii}$ [9]:

$$\widehat{\Psi}^{[n]}_{I,i}(\mathbf{x}) = \Psi^{[n]}_{I,i}(\mathbf{x}) + \mathbf{H}^{[n-1]}(\mathbf{x}) \boldsymbol{\xi}_{Ii} \Theta_I(\mathbf{x}) \tag{27}$$

where

$$\Theta_I(\mathbf{x}) = \begin{cases} 1 & \text{if } \mathbf{x} \in \text{supp}(\Psi_I^{[n]}(\mathbf{x})) \\ 0 & \text{if } \mathbf{x} \notin \text{supp}(\Psi_I^{[n]}(\mathbf{x})) \end{cases}. \tag{28}$$

Inserting the test functions (27) into (25) yields the linear systems of equations

$$\begin{aligned} &\mathbf{A}_I \boldsymbol{\xi}_{1I} = \mathbf{r}_{I1} \\ &\vdots \\ &\mathbf{A}_I \boldsymbol{\xi}_{Id} = \mathbf{r}_{Id} \end{aligned} \tag{29}$$

where

$$\begin{aligned} \mathbf{A}_I &= \overset{\wedge}{\int_\Omega} \mathbf{H}^{[n-1]}(\mathbf{x}) \{\mathbf{H}^{[n-1]}\}^{\mathrm{T}}(\mathbf{x}) \Theta_I(\mathbf{x} - \mathbf{x}_I) \mathrm{d}\Omega, \\ \mathbf{r}_{Ii} &= \overset{\wedge}{\int_{\partial\Omega}} \Psi_I^{[n]}(\mathbf{x}) \mathbf{H}^{[n-1]}(\mathbf{x}) n_i(\mathbf{x}) \mathrm{d}\Gamma - \overset{\wedge}{\int_\Omega} \Psi_I^{[n]}(\mathbf{x}) \mathbf{H}_{,i}^{[n-1]}(\mathbf{x}) \mathrm{d}\Omega \\ &- \overset{\wedge}{\int_\Omega} \Psi_{I,i}^{[n]}(\mathbf{x}) \{\mathbf{H}^{[n-1]}\}^{\mathrm{T}}(\mathbf{x}) \mathrm{d}\Omega. \end{aligned} \tag{30}$$

The type of numerical integration is unspecified, and the framework allows construction of test functions variationally consistent with, for example, direct nodal integration, SCNI (for higher order exactness) and SNNI.

The nodal integration of the weak form with variationally consistent integration can be written as:

$$\widehat{\mathbf{K}}\mathbf{u} = \mathbf{f} \tag{31}$$

where

$$\begin{aligned} \widehat{\mathbf{K}} &= \sum_{L \in \mathcal{Z}} \widehat{\mathbf{B}}^{\mathrm{T}}(\mathbf{x}_L) \mathbf{B}(\mathbf{x}_L) W_L, \\ \widehat{\mathbf{B}}(\mathbf{x}_L) &= \begin{bmatrix} \widehat{\Psi}_{1,1}^{[n]}(\mathbf{x}_L) & \widehat{\Psi}_{2,1}^{[n]}(\mathbf{x}_L) & \dots & \widehat{\Psi}_{N_P,1}^{[n]}(\mathbf{x}_L) \\ \vdots & & & \vdots \\ \widehat{\Psi}_{1,d}^{[n]}(\mathbf{x}_L) & \widehat{\Psi}_{2,d}^{[n]}(\mathbf{x}_L) & \dots & \widehat{\Psi}_{N_P,d}^{[n]}(\mathbf{x}_L) \end{bmatrix}. \end{aligned} \tag{32}$$

4 Numerical Examples

In this section the relative performance of the meshfree Galerkin and Strong Form Collocation methods discussed in Sect. 3 is examined numerically. The minimum order of approximation required for convergence is employed for each method: for Galerkin methods the minimum is linear, while for Strong Form Collocation the order is quadratic [28]. The studies show that due to the reduced performance of Strong Form Collocation under collocation at nodes (versus using more collocation points), and the superconvergence observed in the gradient smoothing Galerkin methods, both are competitive in terms of rates of convergence and accuracy and yield a "fare" comparison. In Galerkin methods, the uniformity of the domain influences the solution accuracy and rate of convergence, so both cases of uniform and non-uniform discretizations are tested. The nodal integration methods in Sect. 3.3 are employed for the Galerkin method, while direct collocation at the nodes is employed for collocation of the strong form as described in Sect. 3.2. Table 1 summarizes the nomenclature and abbreviations used in the numerical examples.

4.1 Performance of Galerkin and Collocation Methods: Uniform Discretization

Consider the Poisson equation (8) with $\Omega: (-1,1)\times(-1,1)$, $\partial\Omega^g = \partial\Omega$ and the prescribed conditions $s = \sin(\pi x)\,\sin(\pi y)$ and $g = 0$. The exact solution of this problem is

$$u = -\frac{1}{2\pi^2}\,\sin(\pi x)\sin(\pi y). \tag{33}$$

The problem is solved using linear RK approximations in the Galerkin method and quadratic RK approximations in the Strong Form Collocation method, with cubic B-spline kernels employed with normalized dilations of 1.75 and 2.75,

Table 1 Method nomenclature used in numerical examples

Formulation	Method	Abbreviation	
		Standard	Variationally consistent
Galerkin weak form	Direct nodal integration	DNI	VC-DNI
	Stabilized conforming nodal integration	SCNI	SCNI (no correction needed)
	Stabilized non-conforming nodal integration	SNNI	VC-SNNI
Strong Form Collocation	Direct collocation	DC	DC (passes patch test)

respectively. The domain is discretized uniformly by 36, 121, 441, and 1681 nodes for a convergence study.

The methods discussed in Sect. 3 are employed for the solution of the problem. However, in uniform discretizations the VC methods perform just as well as the non-corrected counterparts in most situations [9], so only the latter are considered in this example. Figure 3 shows the error plotted against the nodal spacing h for each of the methods. It can be seen that all Galerkin methods yield optimal convergence rates of 2.0 in the L^2 norm and 1.0 in the H^1 semi-norm, with the gradient smoothing methods SCNI and SNNI achieving superconvergent rates in derivatives. The direct collocation (DC) in the Strong Form Collocation method exhibits rates in the L^2 norm lower than optimal of 3.0 for the quadratic basis employed. This can be attributed to the low accuracy of using very few collocation points which can be explained by the equivalent least-squares residual of the Strong Form Collocation method [29]. Because of these two observed trends, the rates of convergence in nodal integration of the Galerkin method with linear basis and collocation of the strong form at nodes with quadratic basis seem comparable.

Now comparing the Galerkin methods and the Strong Form Collocation methods in terms of effectiveness (CPU time versus error), it can be seen in Fig. 4 that the Galerkin methods are the most effective in the L_2 norm, although for the solution derivatives, DC and SNNI perform similarly while others are less effective, with DNI the least effective. Overall, considering both norms, the Galerkin method with SCNI and SNNI are the most effective methods in uniform discretizations, with collation using DC a close competitor.

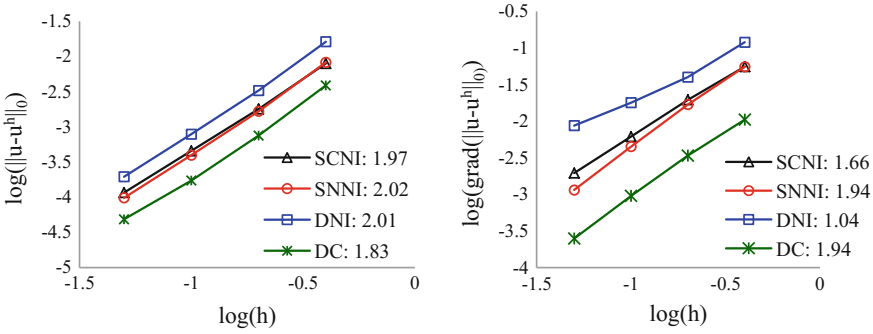

Fig. 3 Convergence of nodal Galerkin method with linear bases (SCNI, SNNI, DNI) and Strong Form Collocation with quadratic bases with direct collocation (DC) under a uniform discretization

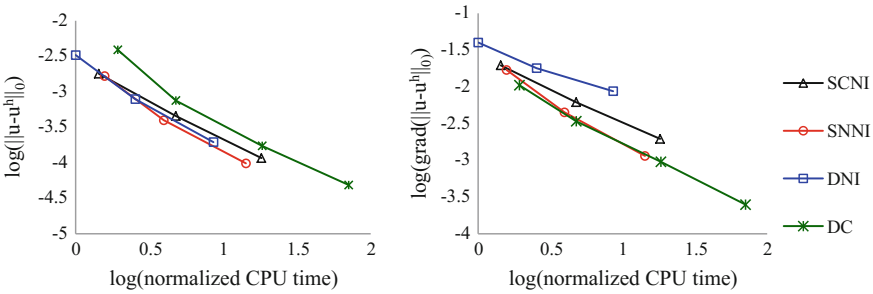

Fig. 4 Relative performances of nodal Galerkin and collocation methods under uniform discretizations

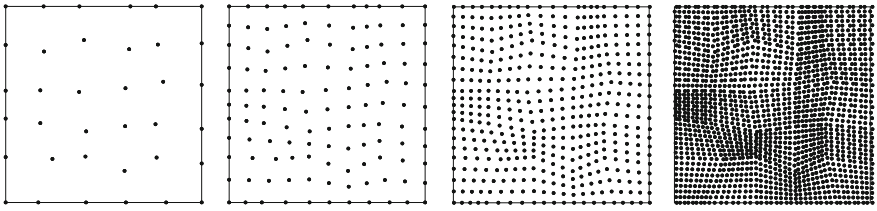

Fig. 5 Refinements for convergence test in non-uniform discretizations

4.2 Performance of Galerkin and Collocation Methods: Non-uniform Discretization

The solutions by meshfree Galerkin methods are particularly sensitive to the uniformity of the discretization. Thus, to truly evaluate the performance of the methods discussed, non-uniform discretizations must also be considered in a convergence study. The boundary value problem and discretization described in the previous example are again employed, except the non-uniform node distributions shown in Fig. 5 are used in place of the uniform discretizations.

As expected, the convergence rates of the VC methods are far superior to their un-corrected counterparts, yielding optimal rates as shown in Fig. 6. Comparing Figs. 3 and 6, it can be seen that the solution by direct collocation at nodes for Strong Form is not severely affected by the uniformity of the discretization, with only slightly lower rates obtained in both norms. As a result of the lower rate of convergence in DC for Strong Form Collocation with quadratic bases and super-convergence in VC Galerkin Methods with linear bases occurring in this example as well, the rates are again comparable as in the case of uniform discretizations.

When comparing the effectiveness of the methods in terms of error and CPU time, it can be seen in Fig. 7 that the Galerkin VC methods and the Strong Form DC method have similar effectiveness in the L^2 norm. However, due to the lower accuracy in derivatives in VC-DNI, only SCNI, VC-SNNI and DC have

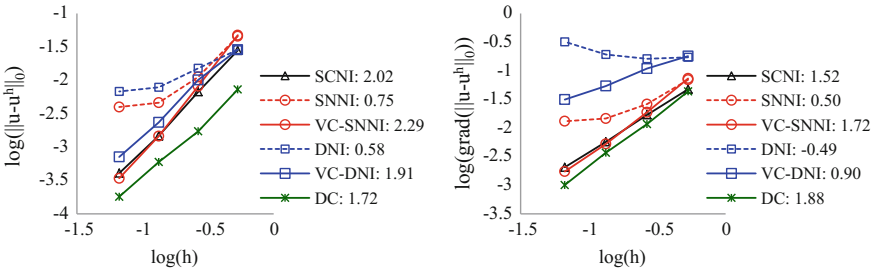

Fig. 6 Convergence of nodal Galerkin method with linear bases (SCNI, SNNI, DNI) and Strong Form Collocation with quadratic bases with direct collocation (DC) under non-uniform discretizations

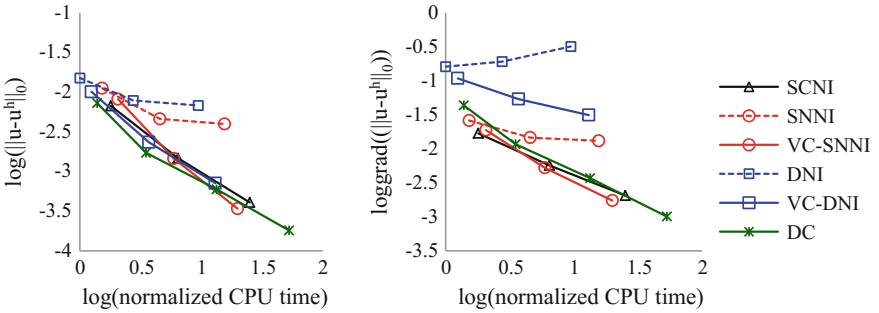

Fig. 7 Relative performances of nodal Galerkin and collocation methods under a non-uniform discretization

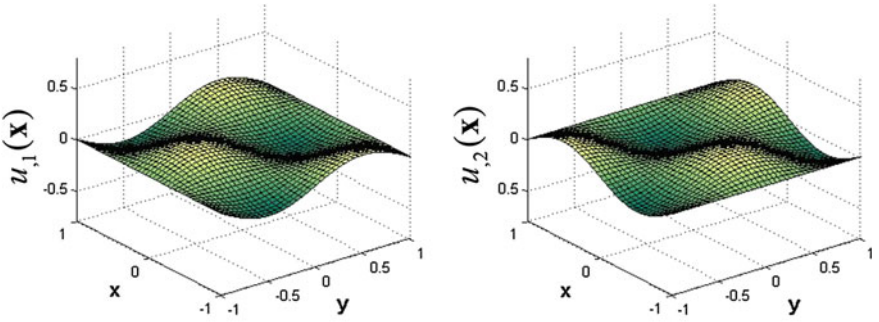

Fig. 8 Derivatives of exact solution

comparable effectiveness in the H^1 semi-norm. The similarity in the performance of these three methods is notable considering the vastly different approaches, including (expensive) higher order derivatives, higher order bases and thus also

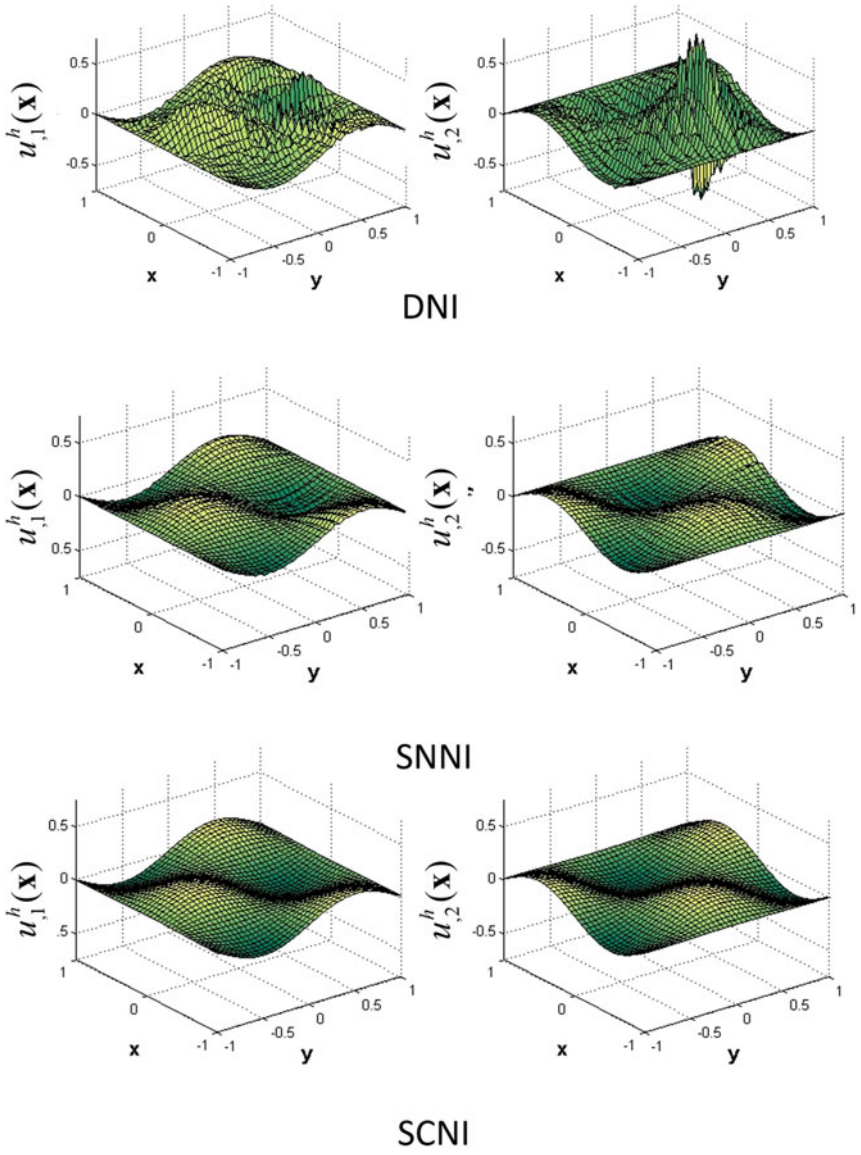

Fig. 9 Solution derivatives obtained by node-based Galerkin and collocation methods

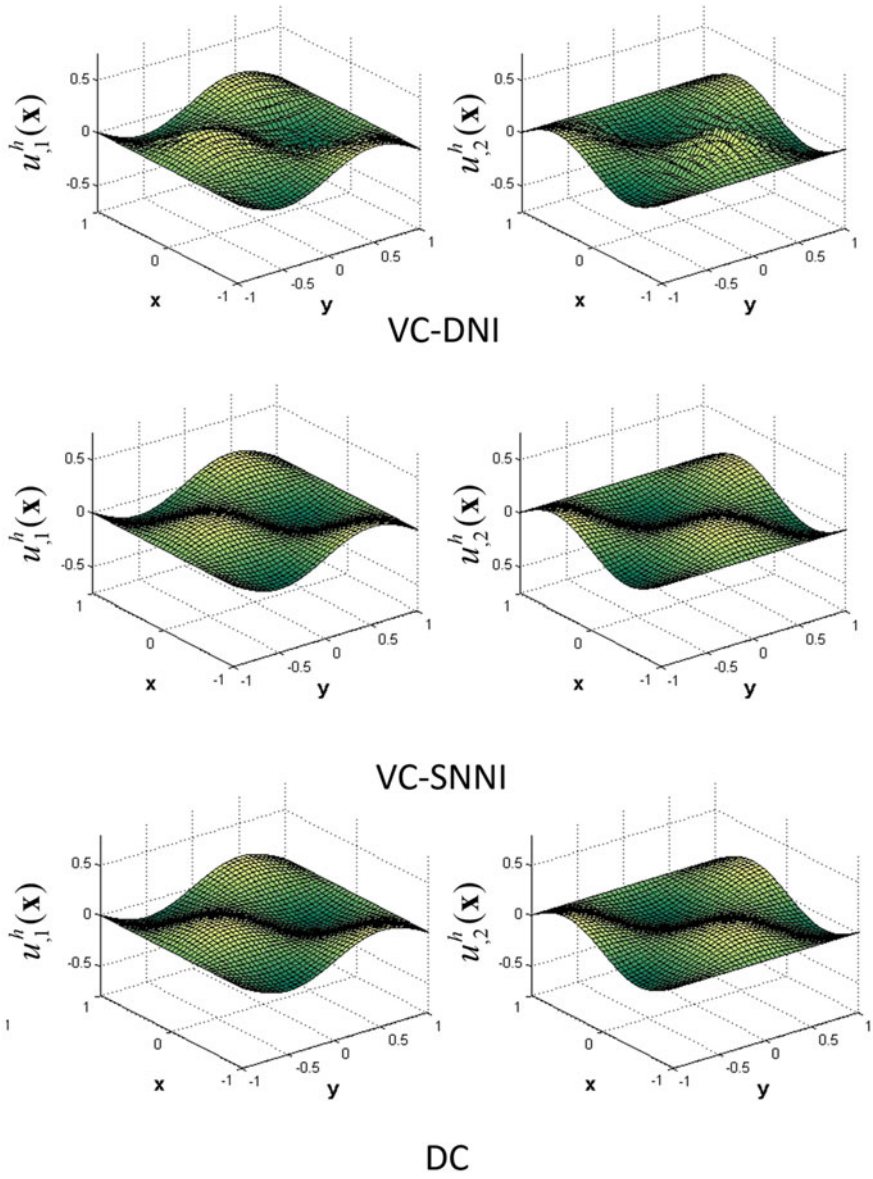

Fig. 9 (continued)

larger dilations employed for Strong Form Collocation. Finally, comparing Figs. 4 and 7, it can be seen that SCNI and VC-SNNI perform the best across both norms of error and both types of discretization, with DC a close competitor.

4.3 *Stability of Node-Based Galerkin and Collocation Methods*

To assess the stability of the methods, we examine the solution derivatives for the last refinement in the previous example. For reference, the derivatives of the exact solution (33) are shown in Fig. 8.

The solution derivatives are shown in Fig. 9 for all the methods considered herein. Several conclusions can be drawn from the Figures. First, it can be seen that the VC correction remarkably stabilizes the solution of the nodally integrated Galerkin method, which has been observed in other contexts as well [17]. However, it is apparent that unstable modes exist in direct nodal integration, which could explain the poorer rates of convergence and poorer levels of error versus the other nodally integrated Galerkin methods. It can also be seen that the VC correction is sufficient to stabilize SNNI, which could explain its apparently good performance in terms of convergence rates and error, yielding solutions similar to SCNI. Finally, the only stable nodally integrated Galerkin methods tested are VC-SNNI and SCNI, while the DC Strong Form Collocation method also gives a stable solution.

5 Conclusions

Several nodal integrations for Galerkin meshfree methods were tested against the purely node-based Strong Form Collocation method. The variationally consistent integration for Galerkin methods yielded optimal convergence rates associated with the linear approximations employed as expected, correcting their counterparts' deficiencies in convergence. However for direct nodal integration, even with the variationally consistent correction, the error in several cases was larger than all other methods indicating it is not a "competitive" method for nodal integration, at least without additional treatment for the stabilization which was not investigated here. In the case of the smoothed gradient VC methods (SCNI, VC-SNNI), superconvergent rates above those associated with linear bases were observed in the numerical examples. For the Strong Form Collocation method with collocation at nodes and quadratic basis, suboptimal convergence rates were observed. As a result, the convergence rates of the direct collocation method for Strong Form with quadratic bases and the smoothed, variationally consistent nodally integrated Galerkin methods with linear bases were similar in all examples. On the other hand, the error was in general always lower for the direct collocation method in the Strong Form method.

In terms of effectiveness, the first conclusion that can be drawn is that VC Galerkin methods are always more effective in the general setting when considering the possibility of non-uniform discretizations. Direct nodal integration for the Galerkin method in general performed more poorly than other methods even with a correction for variational consistency, and again can be considered not "competitive" with the other methods tested. Despite yielding lower error, the Strong Form with direct collocation did not always perform as well as the Galerkin method with SNNI and SCNI in terms of efficiency in uniform discretizations. In the case of non-uniform discretizations, Galerkin methods with VC-SNNI and SCNI performed closely to direct collocation of the strong form at nodes. Considering both uniform and non-uniform discretizations, VC-SNNI and SCNI seem to be the most effective methods tested. That is, for a given level of error, they yield the least CPU time, and for a given CPU time, these methods will yield the least amount of error.

The stability of the solutions obtained by the Galerkin and Strong Form Collocation method was also investigated. First, variationally consistent integration corrected instabilities observed in DNI and SNNI. It could not however, completely remove the unstable modes in DNI, which is possibly why it was not competitive compared to other methods as the error in the derivatives was large due to the instability. Comparison of stabilized direct nodal integration, such as naturally stabilized nodal integration [19] was beyond the scope of this study but warrants investigation, particularly since SCNI and SNNI also require additional treatments to remain stable in certain special situations. As a result of the stabilizing effect of the VC corrections, VC-SNNI yielded stable solutions, and SCNI and VC-SNNI were the only Galerkin methods that did not exhibit instability.

Direct collocation of the strong form also did not yield an instability. It would appear that in contrast to Galerkin methods, collocation methods do not suffer from instability when evaluating the 2nd order derivatives at nodal locations, and do not require special treatment in this case.

Overall, the numerical examples showed that the smoothed gradient, variationally consistent nodal integration for the Galerkin method performed very similar to direct collocation of the strong form at the nodes. Both yielded similar rates of convergence and effectiveness, and all three methods did not show instability in the numerical solution. However, direct collocation in some cases was not as effective, and therefore, although all competitive, the smoothed Galerkin methods with variational consistency yielded the most effective solution techniques.

There is also a striking similarity between the behavior of variationally consistent smoothed gradient Galerkin methods, SCNI and VC-SNNI. However, as a non-conforming method, VC-SNNI has the advantage of dispensing of conforming cells which has several implications, such as using VC-SNNI for ease of implementation, or for solving extremely large deformation problems where non-conforming smoothing is more effective. On the other hand, SCNI has the advantage of yielding a symmetric system of equations, and this feature can also be leveraged in the choice of solver. Future work will investigate the effectiveness of other stabilized nodal integrations, as well as background collocation and background integration, comparing them to the methods discussed in this work.

References

1. J.S. Chen, C. Pan, C.-T. Wu, W.K. Liu, Reproducing Kernel particle methods for large deformation analysis of non-linear structures. Comput. Methods Appl. Mech. Eng. **139**(1–4), 195–227 (1996)
2. J.-S. Chen, C. Pan, C.-T. Wu, Large deformation analysis of rubber based on a reproducing kernel particle method. Comput. Mech. **19**(3), 211–227 (1997)
3. J.-S. Chen, C. Pan, C.M.O.L. Roque, H.-P. Wang, A Lagrangian reproducing kernel particle method for metal forming analysis. Comput. Mech. **22**(3), 289–307 (1998)
4. P.C. Guan, J.S. Chen, Y. Wu, H. Teng, J. Gaidos, K. Hofstetter, M. Alsaleh, Semi-Lagrangian reproducing kernel formulation and application to modeling earth moving operations. Mech. Mater. **41**(6), 670–683 (2009)
5. S.-W. Chi, C.-H. Lee, J.-S. Chen, P.-C. Guan, A level set enhanced natural kernel contact algorithm for impact and penetration modeling. Int. J. Numer. Methods Eng. **102**(3–4), 839–866 (2015)
6. Y. You, J.-S. Chen, H. Lu, Filters, reproducing kernel, and adaptive meshfree method. Comput. Mech. **31**(3), 316–326 (2003)
7. T. Rabczuk, T. Belytschko, Adaptivity for structured meshfree particle methods in 2D and 3D. Int. J. Numer. Methods Eng. **63**(11), 1559–1582 (2005)
8. S. Li, W.K. Liu, Meshfree and particle methods and their applications. Appl. Mech. Rev. **55** (1), 1–34 (2002)
9. J.S. Chen, M. Hillman, M. Rüter, An arbitrary order variationally consistent integration for Galerkin meshfree methods. Int. J. Numer. Methods Eng. **95**(5), 387–418 (2013)
10. T. Belytschko, Y. Guo, W.K. Liu, S.P. Xiao, A unifieded stability analysis of meshless particle methods. Int. J. Numer. Methods Eng. **48**(9), 1359–1400 (2000)
11. T. Belytschko, Y.Y. Lu, L. Gu, Element-free Galerkin methods, Int. J. Numer. Methods Eng. **37**, April 1993, 229–256, (1994)
12. S.R. Beissel, T. Belytschko, Nodal integration of the element-free Galerkin method. Comput. Methods Appl. Mech. Eng. **139**, 49–74 (1996)
13. J. Bonet, S. Kulasegaram, Correction and stabilization of smooth particle hydrodynamics methods with applications in metal forming simulations. Int. J. Numer. Methods Eng. July 1998, 1189–1214, (2000)
14. J.-S. Chen, C.-T. Wu, S. Yoon, A stabilized conforming nodal integration for Galerkin mesh-free methods, Int. J. Numer. Methods Eng. **207**, February 2000, 435–466 (2001)
15. I. Babuška, U. Banerjee, J.E. Osborn, Q. Li, Quadrature for meshless methods. Int. J. Numer. Methods Eng. **76**(9), 1434–1470 (2008)
16. S.N. Atluri, T.L. Zhu, A new meshless local Petrov-Galerkin (MLPG) approach to nonlinear problems in computer modeling and simulation. Comput. Model. Simul. Eng. **3**(3), 187–196 (1998)
17. M. Hillman, J.-S. Chen, S.-W. Chi, Stabilized and variationally consistent nodal integration for meshfree modeling of impact problems. Comp. Part. Mech. **1**, 245–256 (2014)
18. C.-T. Wu, M. Koishi, W. Hu, A displacement smoothing induced strain gradient stabilization for the meshfree Galerkin nodal integration method, Comput. Mech. (2015)
19. M. Hillman, J.S. Chen, An accelerated, convergent, and stable nodal integration in Galerkin meshfree methods for linear and nonlinear mechanics. Int. J. Numer. Methods Eng. **107**, 603–630 (2016)
20. P.W. Randles, L.D. Libersky, Normalized SPH with stress points, Int. J. Numer. Methods Eng. **48**, May 1999, 1445–1462 (2000)
21. T. Rabczuk, T. Belytschko, S.P. Xiao, Stable particle methods based on Lagrangian kernels. Comput. Methods Appl. Mech. Eng. **193**(12–14), 1035–1063 (2004)
22. T. Nagashima, Node-By-Node Meshless Approach and Its Applications to Structural Analyses, vol. 385, April 1997, pp. 2–3, (1999)

23. G.-R. Liu, G.Y. Zhang, Y.Y. Wang, Z.H. Zhong, G.Y. Li, X. Han, A nodal integration technique for meshfree radial point interpolation method (NI-RPIM). Int. J. Solids Struct. **44** (11–12), 3840–3860 (2007)
24. J.-S. Chen, W. Hu, M.A. Puso, Y. Wu, X. Zhang, Strain smoothing for stabilization and regularization of galerkin meshfree methods. Lect. Notes Comput. Sci. Eng. **57**, 57–75 (2007)
25. D. Wang, J. Wu, An efficient nesting sub-domain gradient smoothing integration algorithm with quadratic exactness for Galerkin meshfree methods. Comput. Methods Appl. Mech. Eng. **298**, 485–519 (2016)
26. E.J. Kansa, Multiquadrics—a scattered data approximation scheme with applications to computational fluid-dynamics—I surface approximations and partial derivative estimates. Comput. Math. with Appl. **19**(8), 127–145 (1990)
27. E. Oñate, S.R. Idelsohn, O.C. Zienkiewicz, R.L. Taylor, A finite point method in computational mechanics. Applications to convective transport and fluid flow, Int. J. Numer. Methods Eng. 39, December 1995, 3839–3866 (1996)
28. H.-Y. Hu, C.-K. Lai, J.-S. Chen, A study on convergence and complexity of reproducing kernel collocation method. Interact. Multiscale Mech. **2**(3), 295–319 (2009)
29. H.-Y. Hu, J.-S. Chen, W. Hu, Weighted radial basis collocation method for boundary value problems. Int. J. Numer. Methods Eng. **69**(13), 2736–2757 (2007)
30. H.-Y. Hu, J.-S. Chen, W. Hu, Error analysis of collocation method based on reproducing kernel approximation. Numer. Methods Partial Differ. Equ. **27**(3), 554–580 (2011)
31. S.-W. Chi, J.-S. Chen, H.-Y. Hu, J.P. Yang, A gradient reproducing kernel collocation method for boundary value problems. Int. J. Numer. Methods Eng. **93**(13), 1381–1402 (2013)
32. W.K. Liu, S. Jun, Y.F. Zhang, Reproducing kernel particle methods. Int. J. Numer. Methods Fluids. **20**(8–9), 1081–1106 (1995)
33. W.K. Liu, S. Li, T. Belytschko, Moving least-square reproducing kernel methods (I) Methodology and convergence. Comput. Methods Appl. Mech. Eng. **143**(1–2), 113–154 (1997)